Applied Ocean Research 38 (2012) 64–73

Contents lists available at SciVerse ScienceDirect

Applied Ocean Research

journal homepage: www.elsevier.com/locate/apor

Lagrangian coupling two-phase flow model to simulate current-induced scour beneath marine pipelines

Morteza Zanganeh[a], Abbas Yeganeh-Bakhtiary[a,b,*], Ahmad Khairi Abd Wahab[c]

[a] School of Civil Engineering, Iran University of Science and Technology (IUST), Tehran, Iran
[b] Hydro-environmental Research Centre, School of Engineering, Cardiff University, Cardiff, Wales, UK
[c] Coastal & Offshore Engineering Institute, Universiti Teknologi Malaysia (UTM), International Campus, Kuala Lumpur, Malaysia

ARTICLE INFO

Article history:
Received 25 September 2011
Received in revised form 4 July 2012
Accepted 17 July 2012

Keywords:
Lagrangian coupling
Marine pipelines
Scour
Soft contact
SPH
SPS model
Two-phase flow

ABSTRACT

This paper presents a Lagrangian coupling two-phase flow model for simulating scour processes beneath a marine pipeline with respect to the sediment and fluid phase interactions. Smoothed Particle Hydrodynamics (SPH) capability is employed to simulate sediment and fluid particles movement, respectively as the Newtonian and non-Newtonian fluids in the framework of two-phase flow modeling. The Sub-Particle Scale (SPS) model also is closured to the fluid phase solver to account for the turbulence effects. The soft contact approach is incorporated in the sediment phase to simulate the interparticle collisions during the local scouring. Following to the Lagrangian coupling model development, the current-induced scour beneath a pipe at tunnel erosion and early stages of lee-wake erosion were explored and then compared with the experiments. The obtained results illustrated the efficiency of the proposed two-phase flow model to reproduce the scour profiles evolution up to the early stages of lee-wake erosion. Within the presented model, the parameters such as pressure field and non-dimensional sediment transport rate beneath the pipe were also estimated.

1. Introduction

Estimation of current-induced scour plays a crucial role in designing both offshore and nearshore pipelines used to convey fresh water and crude oil. Recently a lot of research effort has been directed toward a better understanding of the current-induced scour beneath a pipeline laid on erodible seabed. The scour process due to the different interactions between flow field, pipe and erodible bed takes place in three subsequent stages; namely onset of scour, tunnel erosion and lee-wake erosion. The hydrodynamics of tunnel erosion and early stage of lee-wake erosion of scour beneath pipelines is highly complex and important from both applied engineering and sediment transport point of view. During these stages, substantial sediment transport takes place and the main part of the scour hole just below the pipe is generated; consequently, the scour hole immediately beneath the pipe expands extremely fast and a mound of sediment begins to form downstream of the pipe.

Experimental activities have shown that during the tunnel erosion continuing to early stage of lee-wake erosion, the migration of the sediment particles beneath pipelines occurs in a very short period of time, which commonly is resulted by the generation of a gap between the pipe and erodible seabed; the vortex shedding then triggers motion of the dune formed at the rear side of pipe [1]. Numerous studies have been reported so far on experimental modeling of scour beneath pipelines. Most of these studies deal with the experimental modeling based on Buckingham theorem [1,2,3,4,5]. Despite significant advances in the experimental modeling, they have their own limitations in having high cost and constraints of scaling effect in the range of applicable parameters. These limitations make the experimental modeling more suitable to estimate the equilibrium depth of scour. On the other hand, the deficiency with the experimental modeling, along with the rapid advancement in computation capacity, led to the popularity of the numerical methods in the simulation of local scouring.

In the application of the numerical methods usually two disciplines have been employed to capture the scour profiles beneath a pipeline, the so-called single-phase and two-phase models. The single-phase models are categorized as the potential flow models (among others, [6,7,8]) and the viscosity/turbulence based models [9,10,11]. The former models were able to predict the maximum depth of scour and the upstream part of the scour hole, but failed to predict correctly the scour profile due to restrictions in simulating both the wake flow and vortex shedding. In the latter models, (normally accompanied with a turbulence closure model), the scour profile could be determined from the mass balance equation in which the sediment transport rate was estimated based on the shear stress exerted by the flow field. These kinds of models are usually referred to as the

* Corresponding author at: Hydro-environmental Research Centre, School of Engineering, Cardiff University, Cardiff, Wales, UK. Tel.: +44 029 2047 4003; fax: +44 029 2087 4292/School of Civil Engineering, Iran University of Science and Technology (IUST), Tehran, Iran. Tel.: +98 021 7724 0096; fax: +98 021 7724 0096.
E-mail address: yeganeh@iust.ac.ir (Abbas Yeganeh-Bakhtiary).

0141-1187/$ - see front matter © 2012 Elsevier Ltd. All rights reserved
http://dx.doi.org/10.1016/j.apor.2012.07.002

process-based models [12]. The process-based models were successfully used in the simulation of scour profile. However, they have a shortcoming in simulating the early stages of local scour.

The single-phase models usually are not able to consider the interparticle interactions in modeling of the scour process beneath marine pipelines explicitly. Therefore, to cope with this problem more recently, some researchers developed the so-called Euler–Euler two-phase flow approaches to model the scour process as a two-phase flow phenomenon [12,13]. On the other hand, the Euler–Lagrange coupling two-phase flow approach as a new method has been applied by many researchers for the case of sediment transport modeling. This approach in comparison to the introduced Euler–Euler approach [13,14,15,16] has the capability not only to track sediment movement based on Mohr–Coulomb failure criterion but also to consider the interparticle interactions in a more natural way. The deficiency with the Euler–Lagrange method, however, is its inherent one-way behavior in considering the sediment–fluid interactions [16,17,18]. This may limit the application of the Euler–Lagrange models to the hyper-concentrated flow cases and it might be attributed to the difficulties arising from the time averaging scheme of sediment–fluid interaction terms for the mesh based problems.

The Smoothed Particle Hydrodynamics (SPH) is one of the earliest Lagrangian models that was initially introduced by Lucy et al. [19] to simulate the astrological explosions. Later on, Monaghan [20] extended the SPH model to simulate the free surface flow. SPH approach as a pure Lagrangian method accompanied by a sediment closured model has been rarely applied to simulate the two-phase flow phenomena. More recently, Ha et al. [21] applied a CSPH model to simulate water jet penetration in a soil media. In the model, the sediment phase was simulated by adding some extra terms imposing interactions between particles, introducing the artificial viscosity and sediment failure with respect to the Mohr–Coulomb theory.

Until now, to the best knowledge of the authors, no Lagrangian coupling two-phase model based on SPH framework has been reported to simulate the current-induced scour profile beneath a pipe. Therefore, in this study, it is attempted to develop a Lagrangian coupling two-phase flow model for simulation of scour process by confining our focus to the tunnel erosion and early stage of lee-wake erosion. Both the sediment and fluid phase are described respectively as Newtonian and non-Newtonian fluid based on the SPH technique. In order to consider the turbulence effects on flow motion, the so-called Sub-Particle Scale (SPS) [22] model is closured to the developed SPH model for fluid phase, which is deduced from Smagorinsky SGS grid-based model. To account for the interparticle collision effects on scour process, the contacts among the sediment particles are simulated by developing a soft contact model closure to the sediment phase. In our approach, the contact forces are estimated based on the Distinct Element Method (DEM), which is initially introduced by Cundall and Strack [23] in rock mechanics, by activating a spring and dashpot system between the contacting particles. The fluid–sediment interaction is also introduced in the form of SPH formulation. To evaluate the developed two-phase model performance, the numerical result is compared against the experimental data of Mao [1] and Oner et al. [24].

The rest of the paper is organized as follows: Section 2 presents a description of the developed Lagrangian two-phase model. The computational domains and development of the boundary conditions and characteristics are outlined in Section 3. In Section 4, the numerical model validation is presented and then the numerical results for the scour formation are discussed. Section 5 summarizes the main findings of the study and provides a brief discussion concerning the developed Lagrangian two-phase model properties.

2. Two-phase flow formulation

2.1. Governing equations

The SPH model uses the moving computational particles for discretizing the domain of current-induced scour beneath a pipe. The governing equations in Lagrangian forms are considered in terms of the continuity and momentum equations as the following [25,26]:

$$\frac{1}{\rho_f}\frac{\partial \rho_f}{\partial t} + \nabla \cdot \left(\vec{u_f}\right) = 0 \tag{1}$$

$$\frac{d\,\vec{u_f}}{dt} = -\frac{\nabla p_f}{\rho_f} + \vec{g} + \nu_f \nabla^2\,\vec{u_f} + \frac{1}{\rho_f}\nabla \cdot \overline{\overline{\tau_f}} + \vec{f_{fs}} \tag{2}$$

where ρ_f is the fluid density; $\vec{u_f}$ is the fluid velocity; t is the time; ν_f is the fluid kinematic viscosity; g is the gravitational acceleration; p_f is the fluid pressure; $-(1/\rho_f)\nabla p_f$ is the fluid pressure gradient term; $\nu_f \nabla^2\,\vec{u_f}$ is the fluid viscous term; $(1/\rho_f)\nabla \cdot \overline{\overline{\tau_f}}$ indicates the fluid large eddy effects; and $\vec{f_{fs}}$ is the sediment–fluid interaction term:

$$\frac{1}{\rho_s}\frac{\partial \rho_s}{\partial t} + \nabla \cdot \left(\rho_s\,\vec{u_s}\right) = 0 \tag{3}$$

$$\frac{d\,\vec{u_s}}{dt} = -\frac{\nabla p_s}{\rho_s} + \vec{g} + \nu_s \nabla^2\,\vec{u_s} - \vec{f_{fs}} + \vec{f_{colp}} \tag{4}$$

where ρ_s is the sediment phase density; p_s is the sediment phase pressure; $\vec{u}_s$ is the sediment phase velocity vector; t is time marching; ν_s is the sediment phase kinematic viscosity; $\nu_s \nabla^2\,\vec{u}$ is the sediment phase viscous force; $\vec{f}_{fs}$ is the sediment–fluid interaction force; and $\vec{f_{colp}}$ is the sediments interparticle force.

In the SPH approximation, each characteristic like $A(\vec{r})$ is estimated by the following integral interpolants equation:

$$A\left(\vec{r}\right) = \int A\left(r'\right) W\left(\vec{r} - \vec{r'}, h\right) dr' \tag{5}$$

where r is the particle position; h is the smoothing length; and $W(\vec{r} - \vec{r'}, h)$ is the weighting or kernel function specified by a Quintic function as

$$W(r,h) = \frac{7}{4\pi h^2}\left(1 - \frac{q}{2}\right)^4 (2q+1) \tag{6}$$

where $q = r/h$. The Quintic kernel function is selected here in order to have no tension instability difficulty compared with the Gaussian, Quadratic and/or Cubic spline kernel functions. Eq. (5) in its discretized form can be expressed as

$$A_m\left(\vec{r}\right) = \sum_j m_{mj}\frac{A_{mj}}{\rho_{mj}} W_{ij} \tag{7}$$

where m_j and ρ_j respectively denote the mass and density of domain particle j; the subscripts m (f and s) represent the fluid and sediment phases, respectively; $W_{ij} = W(\vec{r_i} - \vec{r_j})$ is the weight function that should be continuous, non-zero within the influence domain (a circle with radius of $2h$). It is noted that the summation is performed all over the particles within the region of influence domain. Moreover, the function should meet the normalization condition ($\int W(\vec{r} - \vec{r'}, h)dr' = 1$) and tends to Dirac delta as the smoothing length, h, tending to zero.

As Ting et al. [27] pointed out, the turbulence effect has a great influence on the fluid flow; therefore, the Sub-Particle Scale (SPS) turbulence closure model was also employed to take the turbulent effects into account as follows:

$$\frac{d\rho_f}{dt} = -\sum_{b=1}^{N} m_b\left(u_f - u_b\right)\vec{\nabla}_f\, W_{fb} \tag{8}$$

$$\frac{d\rho_s}{dt} = -\sum_{j=1}^{N} m_b (u_s - u_j)\, \vec{\nabla}_s W_{sj} \tag{9}$$

$$\frac{d\vec{u}_f}{dt} = -\sum_{b=1}^{N} m_b \left(\frac{p_f}{\rho_f^2} + \frac{p_b}{\rho_b^2}\right) \vec{\nabla}_f W_{fb} + \sum_{b=1}^{N} m_b \left(\frac{4\nu_f \vec{r}_{fb}\vec{u}_{fb}}{(\rho_f + \rho_b)\left|\vec{r}_{lb}\right|^2}\right) \vec{\nabla}_f W_{fb} + \sum_{b=1}^{N} m_b \left(\frac{\tau_f^{\alpha\beta}}{\rho_f^2} + \frac{\tau_b^{\alpha\beta}}{\rho_b^2}\right) \vec{\nabla}_f W_{fb} + \vec{g} - \vec{f}_{fs} \tag{10}$$

$$\frac{du_s}{dt} = -\sum_{j=1}^{N} m_b \left(\frac{p_s}{\rho_s^2} + \frac{p_j}{\rho_j^2}\right) \vec{\nabla}_s W + \sum_{j=1}^{N} m_b \left(\frac{4\nu_s \vec{r}_{sj}\vec{u}_{sj}}{(\rho_s + \rho_j)\left|\vec{r}_{sj}\right|^2}\right) \vec{\nabla}_s W_{sj} + \vec{g} + \vec{f}_{fs} + \vec{f}_{colp} \tag{11}$$

where $\tau^{\alpha\beta}/\rho = 2\nu_t S_{\alpha\beta} - (2/3)k\delta_{\alpha\beta} - (2/3)C_l \Delta l^2 \delta_{\alpha\beta}|S_{\alpha\beta}|^2$ is the sub-particle stress tensor; $\nu_t = [\min(C_s\Delta l)]^2|S|$ is the turbulence eddy viscosity; k is the SPS turbulence kinetic energy; C_s is the Smagorinsky constant (0.12); $C_l = 0.0066$; Δl is the particle–particle spacing; $|S| = \sqrt{(2S_{\alpha\beta}S_{\alpha\beta})}$, $S_{\alpha\beta}$ is the SPS strain tensor; and $\delta_{\alpha\beta}$ is the Dirac delta coefficient. Subscripts f and b represented the fluid particles; whereas, s and j denoted the sediment particles.

Incompressibility approximation in the SPH method is a common trick to replace a stiff equation of state rather than solving the Poisson's equation. This equation relates the density and the pressure for both sediment and fluid particles as

$$P_m = \frac{c_{0m}^2 \rho_{0m}}{7}\left(\left(\frac{\rho_m}{\rho_{0m}}\right)^7 - 1\right) \tag{12}$$

where m denotes the kind of particle (sediment or fluid); $c_{0m} = \sqrt{\partial p/\partial \rho}$, coefficient of sound speed, herewith $c_{0m} = 10u_{max}$ was used to keep Mach number less than 0.1, meaning that the compressibility is negligible and u_{max} is the maximum velocity of particles.

In the flow with the sharp fluid interfaces, a spurious pressure fluctuation brings an incorrect pressure approximation to SPH. To resolve the problem of spurious pressure fluctuation, some remedies have been proposed. Colagrossi and Landrini [28] employed a moving-least-square kernel approximation to re-initialize the density field at distinctive time steps to get more accurate pressure field. Khayyer and Gotoh [29,30] derived a more accurate source term of a Poisson pressure equation based on a higher order calculation of the time rate for changing of density rather than the density itself in the ISPH and MPS, respectively. More recently, a modified Poisson pressure equation along with a corrective matrix for pressure gradient is introduced to resolve the spurious pressure fluctuation in MPS by Khayyer and Gotoh [31]. The present study, however, is confined to the current-induced scour beneath a pipe in which the spurious pressure fluctuations are negligible. Hence, the pressure field can be approximated well with filtering or averaging techniques. In other words, the filtering or smoothing techniques act as the artificial damping factors. The smoothing techniques expressed as follows are applied in every 200 time steps [32]:

$$\vec{u}_i^{\,s} = (1-\beta)\,\vec{u}_i + \beta \frac{\sum_j (m_j/\rho_j)\,\vec{u}_i\, W_{ij}}{\sum_j (m_j/\rho_j) W_{ij}} \tag{13}$$

$$\rho_i^s = \frac{\sum_j (m_j/\rho_j)\,\rho_j W_{ij}}{\sum_j (m_j/\rho_j) W_{ij}} \tag{14}$$

$$p_i^s = \frac{\sum_j (m_j/\rho_j)\left[p_j^T + \rho_i g(z_j - z_i)\right] W_{ij}}{\sum_j (m_j/\rho_j) W_{ij}} \tag{15}$$

where $\vec{u}_i^T$ is the updated velocity via explicit integration of the momentum equation; $\vec{u}_i^s$ is the smoothed velocity; β is the smoothing parameter; ρ_i^s is the smoothed density; p_j^T is the updated pressure and p_i^s is the smoothed pressure with hydrostatic correction.

2.2. Interparticle acting forces

The interphase interactions in the developed two-phase flow modeling are categorized as the fluid–sediment interactions and the sediment–sediment or interparticle interactions. The fluid–sediment interactions term can be divided into the drag force, pressure gradient term, and viscous terms. Estimation of these forces on given sediment particle is based on the influence domain concept in which the nearer fluid particles impose more acting force on the considered sediment particle and are estimated as

$$f_{fs} = \sum_{j=1}^{N} W_{ij} \frac{m_f}{\rho_f} C_d \frac{\pi}{4} d_s^2 |u_f - u_j|(u_f - u_j) - \sum_{j=1}^{N} m_f \left(\frac{p_f}{\rho_f^2} + \frac{p_j}{\rho_j^2}\right) \vec{\nabla}_f W_{fj} + \sum_{j=1}^{N} m_f \left(\frac{4\nu_f \vec{r}_{sj}\vec{u}_{fj}}{(\rho_f + \rho_j)\left|\vec{r}_{fj}\right|^2}\right) \vec{\nabla}_s W_{fj} \tag{16}$$

where C_d is the drag force coefficient; d_s is the particle diameter; u_f and u_j are the velocity of fluid and sediment particles, respectively.

A soft contact approach is adapted to estimate the interparticle forces ($\vec{f}_{colp}$), which is initially formulated by Cundall and Strack [23] in the DEM. This approach has been implemented to simulate the interparticle forces activated between each contacting particle [17]. The term of interparticle interactions can be presented as the following by considering a spring–dashpot system between contacting sediments (see Fig. 1):

$$f_{colp} = \begin{bmatrix} \sum_j \{-f_n \cos\alpha_{ij} + f_s \sin\alpha_{ij}\}_j \\ \sum_j \{-f_n \cos\alpha_{ij} + f_s \sin\alpha_{ij}\}_j \end{bmatrix} \tag{17}$$

$$f_n(t) = e_n(t) + d_n(t) \tag{18}$$

$$f_s(t) = e_s(t) + d_s(t) \tag{19}$$

$$e_n(t) = e_n(t - dt) + k_n \cdot \Delta\varsigma_n \tag{20}$$

$$d_n(t) = \frac{\eta_n \cdot \Delta\varsigma_n}{dt} \tag{21}$$

$$e_s(t) = e_s(t - dt) + k_s \cdot \Delta\xi_s \tag{22}$$

$$d_s(t) = \frac{\eta_s \cdot \Delta\xi_s}{dt} \tag{23}$$

Sediment grains were assumed to be non-cohesive particles, and a tangential force limit was utilized in the local tangential direction, whose characteristics can be defined as

$$f_n(t) = f_s(t) = 0 \;if\; e_n(t) < 0 \tag{24}$$

$$f_s(t) = \mu \cdot SIGN[e_n(t), e_s(t)] \;if\; |e_s(t)| > \mu_f e_n(t) \tag{25}$$

where f_n and f_s are the normal and tangential components of the force acting between ith and jth particles on the n–s local coordinate system; α_{ij} is the contacting angle between ith and jth particles; e_n

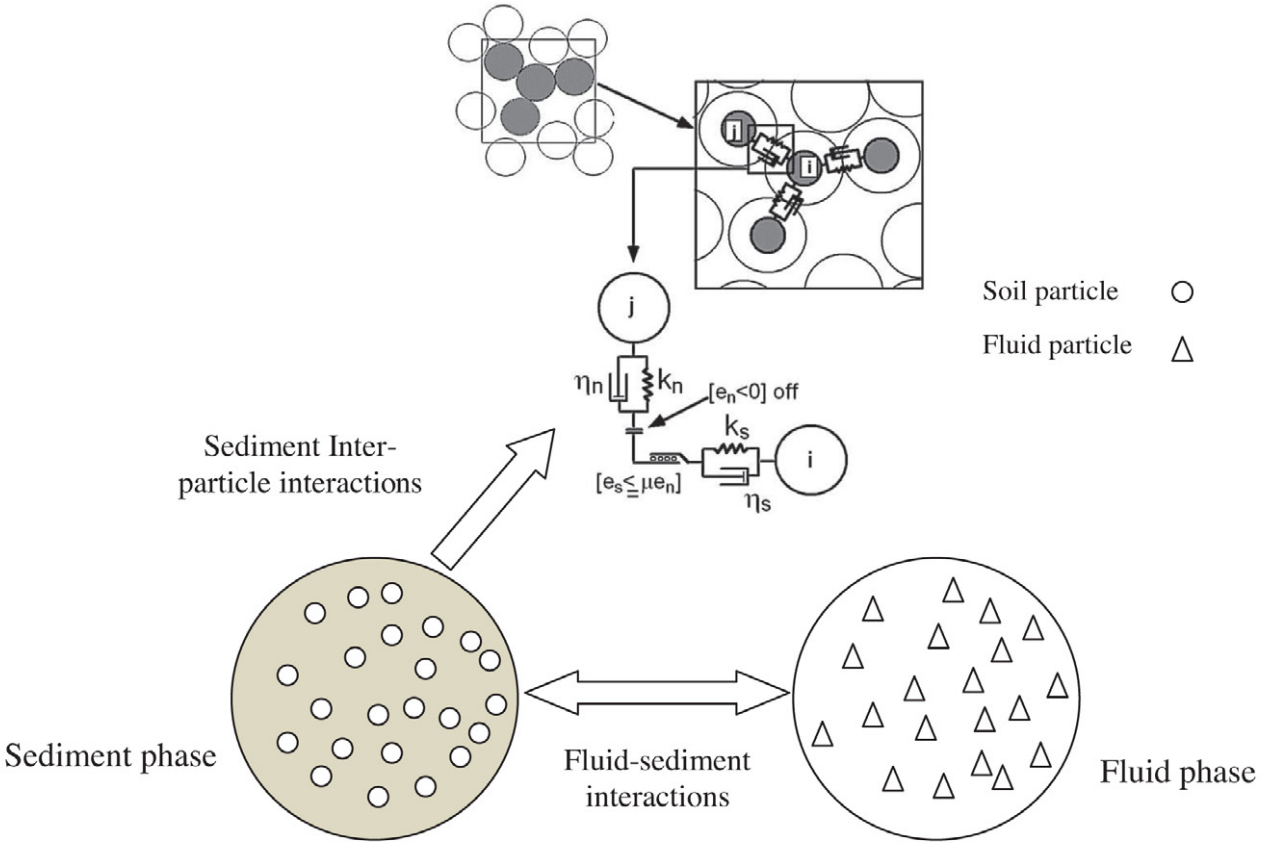

Fig. 1. A spring–dashpot system.

and e_s are the forces acting on the spring; d_n and d_s are the forces acting on the dashpot; k_n and k_s are the spring constants; η_n and η_s are the viscosity constants; $\Delta\zeta_n$ and $\Delta\zeta_s$ are the displacements of a particle during the time increment; μ is the friction coefficient; and the *SIGN* function is defined as:

$$SIGN[x, y] = \begin{cases} +|x| \text{ when } y \geq 0 \\ -|x| \text{ when } y < 0 \end{cases} \tag{26}$$

According to Cundall and Strack [23], to satisfy the stability of the soft contact numerical schemes, time step Δt should be taken as a proportion of the critical time step or Δt_c. Δt_c can be estimated on the basis of a single mass-spring system with a single degree of freedom as

$$\Delta t = \frac{\Delta t_c}{20}; \quad \Delta t_c = 2\pi\sqrt{\frac{m_s}{2k_n}} \tag{27}$$

where m_s is the mass of a sediment particle (for more details please refer to Yeganeh-Bakhtiary et al. [17]).where (x_i, y_i) and (x_j, y_j) are the coordinates of the ith and jth particles; and d_s is the sediment diameter.

To account for the interparticle collisions, as shown in Fig. 1, a system of spring–dashpot is introduced among the sediment particle. In the case of uniform sediment the assessment of contacting particle is formulated as

$$\sqrt{(x_j - x_i)^2 + (y_j - y_i)^2} \leq d_s \tag{28}$$

2.3. Sediment viscosity in non-Newtonian form

Evaluation of the sediment dynamic viscosity (μ_s) as a non-Newtonian fluid is of great importance in the two-phase flow modeling. Therefore, to estimate the value of dynamic viscosity, the so-called Cross model is applied; the relationship among the different parameters can be expressed as follows [33]:

$$\frac{\mu_0 - \mu_s}{\mu_s - \mu_\infty} = (K\dot{\gamma})^{m_1} \tag{29}$$

where μ_0 and μ_∞ are the viscosities at the very low and very high shear rates, respectively; and K and m_1 are the constant parameters. As the sediment phase characteristics is approximated similar to the Bingham or non-Newtonian fluid, the shear stress is decreased under the yield stress condition, and the fluid structure again keeps changing to a plug flow or no flow condition. Consequently, the effective viscosity of a Bingham fluid can be expressed by

$$\mu_s = \frac{\mu_0 + K\mu_\infty\dot{\gamma}}{1 + K\dot{\gamma}} \tag{30}$$

where $\dot{\gamma}$ is the shear rate defined by the second invariant of deformation strain in 2D coordinates:

$$\dot{\gamma} = \sqrt{2\left(\frac{\partial u_{si}}{\partial x}\right)^2 + 2\left(\frac{\partial u_{sj}}{\partial y}\right)^2 + 2\left(\frac{\partial u_{si}}{\partial x} + \frac{\partial u_{sj}}{\partial y}\right)^2} \tag{31}$$

where x and y denote the vertical and the horizontal directions. Following to the presented Lagrangian two-phase flow model formulation, the algorithm of the simulation process of the current-induced

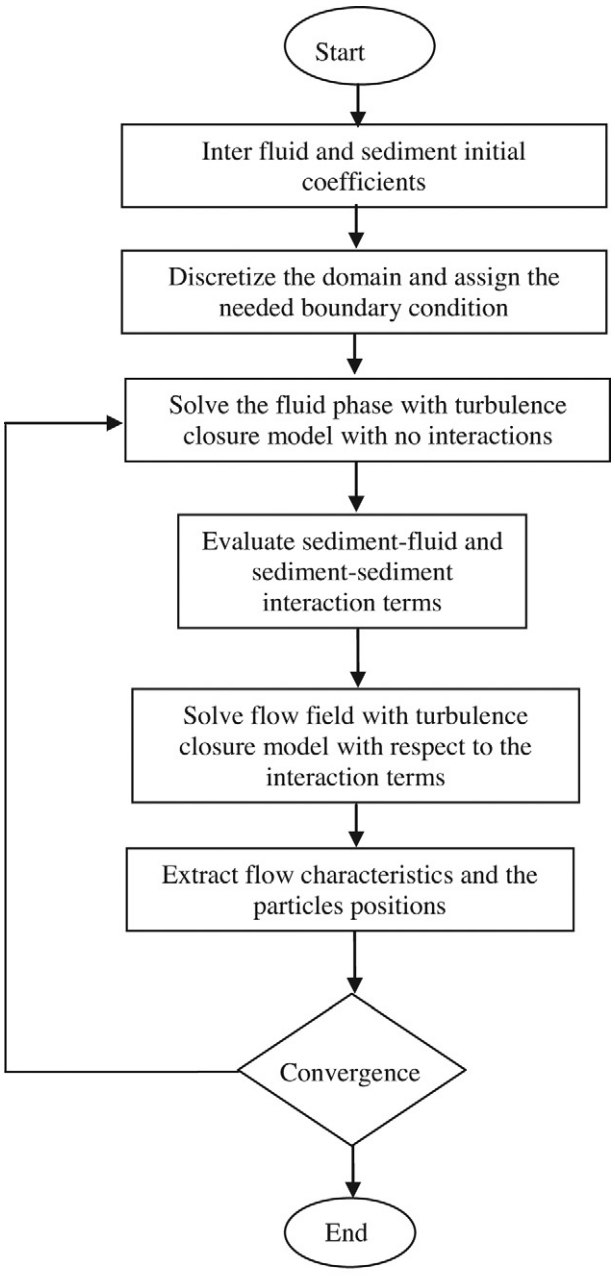

Fig. 2. Flow diagram of the developed two-phase flow model simulation process.

scour beneath a pipe is shown in Fig. 2.

Comparing the above equation with the Bingham model under $K\dot{\gamma} \geq 1$ condition, the other parameters of the Cross model can be defined (see [34] for details):

$$\mu_0 = 0.07\ Ns/m^2, \quad \tau_B = 25\ N/m^2, \quad K = \frac{\mu_0}{\tau_B}, \quad \text{and } \mu_\infty = 10^3\mu_0.$$

3. Computational domain and boundary conditions

The model parameters employed in the simulation are set the same as those used in the experiments of Mao [1], as depicted in Fig. 3. In the studying of scour beneath a pipe, the Mao's experiment has been selected as the benchmark test to evaluate the numerical model performance for scouring beneath a pipe (among others see

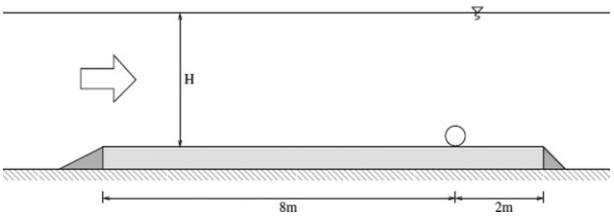

Fig. 3. Sketch of Mao's experimental setup [1].

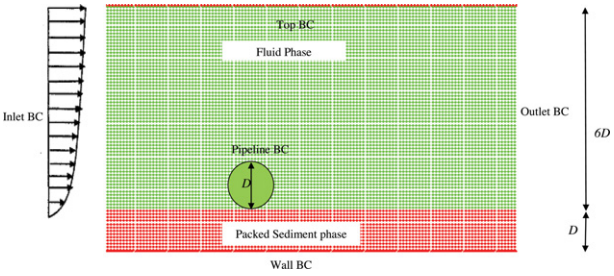

Fig. 4. Considered numerical setup for the two-phase flow model.

[10,12,13]). Fig. 4 shows a sketch of the computational domain of the Lagrangian model for the simulation of scour beneath a pipe with its corresponding boundary conditions. A rectangular computational domain was considered. The simulation was carried out using a packed sand layer with the maximum volumetric sediment concentration as the sediment phase. A small sinusoidal perturbation was introduced to the initial bed profile. In other words, an initial sinusoidal bed shape with a small gap was imposed between the pipe and the bed surface because of the numerical requirements to trigger the sediments motion. The same approach has been adopted by Liang and Cheng [35] and Zhao and Fernando [13], which is a remedy to simulate the tunnel erosion process happening right after the onset of scour. The boundary conditions were classified as the inlet and outlet boundary conditions or the open boundary conditions, the wall boundary condition and the pipeline boundary condition and expressed in the following:

- Periodic boundary

Periodic boundary condition was implemented to simulate the inlet and outlet boundary conditions. In the periodic boundary, when a moving particle passes the outlet boundary of the computational domain, it is reintroduced again from the inlet of the given domain [36]. Furthermore, two ghost domains with similar hydrodynamic characteristics to that of the main computational domain were employed to make up for the lack of influence domain for the lateral particles as plotted in Fig. 5. The mean inlet velocity profile, $U(y)$, was prescribed as a fully developed turbulent velocity profile by assuming the log-law across of the flow domain as follows:

$$\begin{cases} \dfrac{U(y)}{u_*} = \dfrac{yu_*}{\nu} & \dfrac{yu_*}{\nu} \leq 11.63 \\ \dfrac{U(y)}{u_*} = \dfrac{1}{\kappa}\ln\left(9.793\dfrac{yu_*}{\nu}\right) & \dfrac{yu_*}{\nu} > 11.63 \end{cases} \tag{32}$$

where u_* is the shear velocity and κ is the von-Karman constant (0.42).

- Wall boundary

The wall boundary condition was described according to Monaghan and Kos [37]: the external forces exerted on the fluid particles prevents them from penetrating into the boundary wall (see Fig. 6). The force experienced by a moving particle was estimated by the

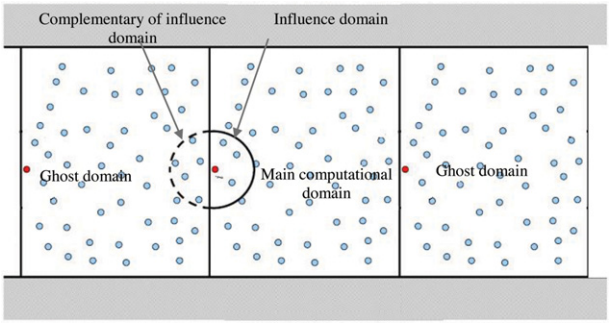

Fig. 5. Sketch of periodic boundary condition.

following expression in the normal direction:

$$\vec{f}\,(X,Y) = \vec{n} \times R(Y) \times P(X) \times \epsilon_Z(z, u_\perp) \tag{33}$$

where $\vec{n}$ is the normal vector of the wall boundary; X and Y are the components of separation between the fluid and boundary particles; $R(Y)$ is the repulsive function; $P(X)$ is a function ensures that a particle is traveling parallel to the wall. The functions $R(Y)$ and $P(X)$ were estimated as follows:

$$R(Y) = \begin{cases} A\dfrac{1}{\sqrt{q}}(1-q), & if\, q < 1 \\ 0 & if\, q \geq 1 \end{cases}; \quad q = \frac{2X}{h} \text{ and } A = \frac{c_i^2}{100h} \tag{34}$$

$$P(X) = \begin{cases} \dfrac{1}{2}\left(1 + \cos\dfrac{\pi X}{\Delta b}\right) & if\, X < \Delta b \\ 0 & \text{otherwise} \end{cases} \tag{35}$$

where Δb is the distance between two adjacent boundary particles; and c_i is the speed of sound corresponding to particle i. Finally, $\epsilon_Z(z, u_\perp)$ is a function to adjust the forces with the water depth and velocity of water particle normal to the boundary and can be calculated as

$$\epsilon_Z(z, u_T) = \epsilon_Z(z) + \epsilon_Z(u_\perp) \tag{36}$$

$$\epsilon_Z(z) = \begin{cases} 0.02 & z \geq 0 \\ |z/h_0| + 0.02 & 0 > z \geq -h_0 \\ 1 & |z/h_0| \geq 0 \end{cases} \tag{37}$$

$$\epsilon_Z(u_\perp) = \begin{cases} 0 & u_\perp > 0 \\ |20u_\perp|/c_0 & |20u_\perp| < c_0 \\ 1 & |20u_\perp| > c_0 \end{cases} \tag{38}$$

where z is the elevation above the local still-water level (h_0). As it is apparent from the above expressions, the only important parameter in this boundary condition is the velocity coefficient usually chosen within the range of 12–40 in the compressible SPH method. Other parameters in Eq. (33) such as $\vec{n}$, $R(Y)$, $P(X)$ and $\epsilon_Z(z, u_\perp)$ can be estimated explicitly according to Monaghan and Kos [37].

- Pipeline boundary

In the Lagrangian model, to introduce the pipe into the computational domain, a special treatment for the wall boundary condition was adopted by adding a new term containing the stress tensor [38]. In other words, the ghost particles near the rigid wall were applied to readily simulate the no-slip wall boundary condition. Contrary to the boundary condition adopted in the Monaghan and Kos [37] study, in this technique the ghost particles were distributed inside the pipeline as a bluff body by assigning an artificial velocity to the boundary particles in the opposite direction of the incident moving particles, as

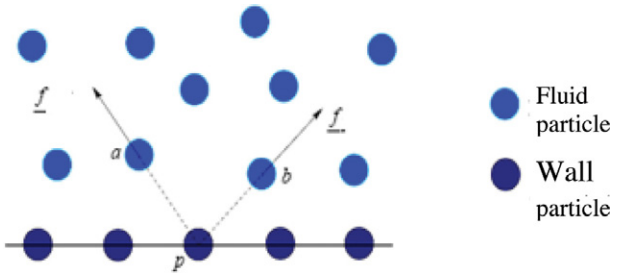

Fig. 6. Particle arrangement in solid wall boundary condition.

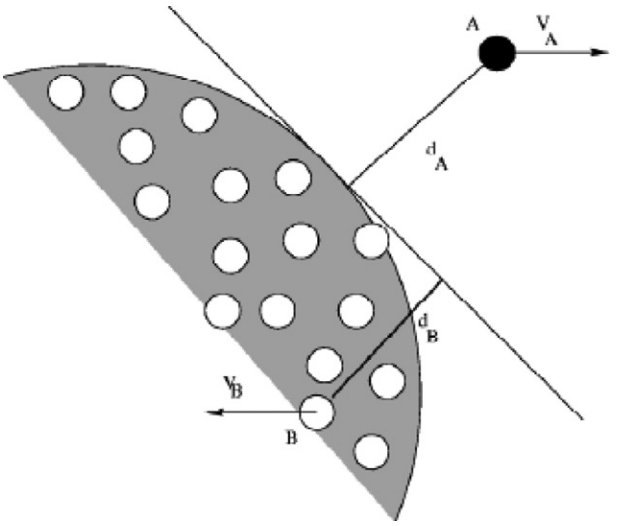

Fig. 7. Treating technique for defining the pipeline boundary condition [39].

shown schematically in Fig. 7. This artificial velocity can be estimated as

$$\vec{u_{fB}} = -\left(\frac{d_B}{d_A}\right)\vec{u_{fA}} \tag{39}$$

where d_i is the minimum distance of a particle from pipe surface; and subscripts A and B representing the fluid and boundary particles, respectively. This feature of boundary particles forces brings extra source terms to the continuity and momentum equations to satisfy the boundary condition:

$$\frac{d\rho_f}{dt} = \sum_{b=1}^{N} m_b\left(\vec{u_f} - \vec{u_b}\right) W_{fb} + \sum_{b=1}^{N_b} m_b\left(\vec{u_f} - \vec{u_b}\right) W_{fb} \tag{40}$$

$$\begin{aligned} \frac{d\vec{u_f}}{dt} &= -\sum_{b=1}^{N} m_b\left(\frac{p_f}{\rho_f^2} + \frac{p_b}{\rho_b^2}\right)\vec{\nabla} W_{fb} \\ &+ \sum_{b=1}^{N} m_b\left(\frac{4v_f\,\vec{r_{lb}}\vec{u_{fb}}}{(\rho_f + \rho_b)\left|\vec{r_{fb}}\right|^2}\right)\vec{\nabla} W_{fb} \\ &+ \sum_{b=1}^{N} m_b\left(\frac{\tau_f^{\alpha\beta}}{\rho_f^2} + \frac{\tau_b^{\alpha\beta}}{\rho_b^2}\right)\vec{\nabla} W_{fb} - \sum_{b=1}^{N_b} m_b\left(\frac{p_f}{\rho_f^2} + \frac{p_b}{\rho_b^2}\right)\vec{\nabla} W_{fb} \\ &+ \sum_{b=1}^{N_b} m_b\left(\frac{4v_f\,\vec{r_{fb}}\vec{u_{fb}}}{(\rho_f + \rho_b)\left|\vec{r_{fb}}\right|^2}\right)\vec{\nabla} W_{fb} + \sum_{b=1}^{N_b} m_b\left(\frac{\tau_f^{\alpha\beta}}{\rho_f^2} + \frac{\tau_b^{\alpha\beta}}{\rho_b^2}\right)\vec{\nabla} W_{fb} + \vec{g} \end{aligned} \tag{41}$$

where N_b is the number of pipe's boundary particles.

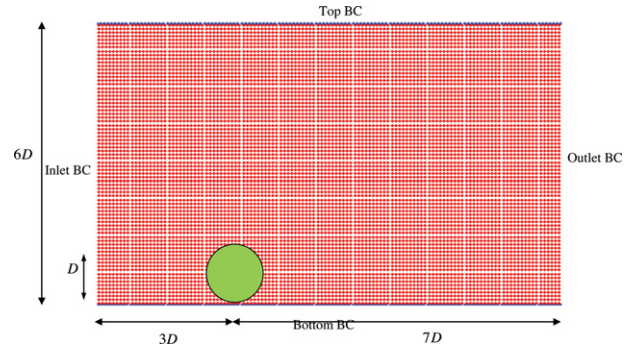

Fig. 8. Sketch of the computational domain in fluid phase model.

Table 1
The SPH fluid phase model parameters in modeling flow pattern around the pipeline.

Characteristic	SPH
Mesh size (m)	0.004
Speed of sound (m/s)	15
Domain dimension	$10D \times 6D$
u_0 (m/s)	0.197
D (cm)	5
Δt (s)	0.00001
Number of particles	9575
β	0.002
Kind of wall boundary condition	Monaghan

4. Results and discussion

4.1. Model verification

One of the most important concerns in developing of a numerical model is its step by step verification. To achieve this, the fluid phase model is validated against Oner et al. [24] experimental study, which measured the current velocity around a pipe located near a rigid bed. The horizontal velocity profiles were registered for different gap to diameter ratios (e/D) including 0.0, 0.2, 0.3 and 1. The model result was evaluated for the test case with a gap ratio of $e/D = 0.0$. In the experimental setup, a transparent Plexiglas-walled flume was used with 1 m width, 0.75 m depth and 14 m length and the pipe was located on a rigid bed. In the chosen case, the pipe diameter and averaged current velocity were respectively 5 cm and 0.197 m/s with the corresponding Reynolds number of $Re_D = 9500$. The computational domain was set to $10D$ long and $6D$ depth as shown in Fig. 8. Particle spacing is 0.004 m and the other parameters related to the numerical setup are reported inTable 1.

Following the numerical model development, the Lagrangian SPH model was exploited to simulate the flow pattern around a pipe. Fig. 9 presents the time-averaged horizontal velocity distribution after 3 s of time marching. As seen, the flow model describes the horizontal velocity profile at the upstream and downstream of the pipe very well; however, it slightly under-predicts the time-averaged velocity around the pipe. A great deal in modeling of scour beneath pipelines is the analysis of flow pattern around a pipe laid on the bed ($e/D = 0.0$). It is concluded that the numerical model results share very good agreement with the Oner et al. [24] experiment and the numerical model is able to estimate the time-averaged velocity with acceptable accuracy.

4.2. Scour simulation

To verify the ability of the Lagrangian two-phase model to simulate current-induced scour, the experiments of Mao [1] were simulated. In Mao's experimental setup, a flume was used with 2 m width, 0.5 m depth and 23 m length; the water depth and the pipe diameter

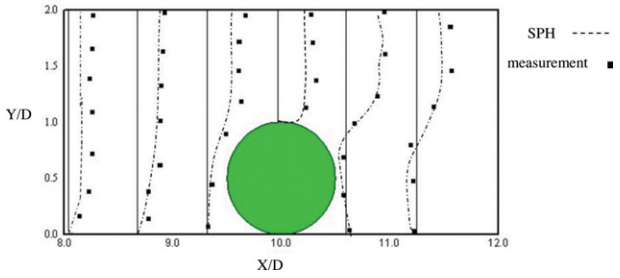

Fig. 9. Time-averaged horizontal velocity for $e/D = 0$, $R_{eD} = 9500$. Compared with Oner et al. [24] observed streamlines.

Table 2
Flow characteristics in two Mao's selected cases.

Pipe diameter (cm)	Shields variable	Sediment average size (mm)	Velocity (m/s)
10	0.065	0.36	0.4
10	0.098	0.36	0.5

Table 3
Constants for the developed two-phase flow model.

β	c_{0m}	C_D	μ	k_n (N/m)	k_s (N/m)	η_n (N s/m)	η_s (N/m)
0.0015	18	0.4	0.57	1×10^6	1×10^5	20	40

were 0.35 m and a pipe with 0.1 m, respectively, and the pipe was placed above a sand layer with average diameter of 0.036 cm. The mean flow velocities were 0.4 m/s for the $\theta = 0.065$ case and 0.5 m/s for the $\theta = 0.098$ case. The selected scour cases were representative of the live-bed scour in the Mao's experiment. Table 2 reports the hydrodynamics conditions of experiments.

The time increment of the calculation for both fluid and sediment phases is adopted as $\Delta t = 0.00001$ s. Table 3 presents the constants used in the Lagrangian two-phase flow model. The spring and dashpot coefficients for estimation of interparticle forces between contacting sediments were estimated from the critical damping conditions (see [17] for more details).

Fig. 10 shows snapshots of the scour profile evolution for the $\theta = 0.065$ case. The only registered profile for this interval in Mao's experiments is shown in Fig. 10(e) corresponding to $t = 6.5$ min. Fig. 10(e) shows a good agreement between the simulated scour profile and the measured scour profile of Mao [1] at $t = 6.5$ min. It can be seen that Fig. 10(b) and (c) represents the typical tunnel erosion situations, where the scour rate is very high and from the beginning of the scour process to 2.5 min a substantial amount of bed particles is pushed away from beneath the pipe. According to Sumer and Fredsøe [4], *large velocities* in the gap between the pipe and bed induce a huge bottom shear stress beneath the pipe that itself results in an intensive sediment transport in the gap, and consequently, a sediment dune forms at the rear side of pipe. Fig. 10(d) and (e) showed that the shape of the scour hole slightly changes from $t = 4.5$ min to $t = 6.5$ min, while the sediment dune starts to move downstream and the early stage of lee-wake erosion may be achieved. After the scour gap was adequately developed, the bottom shear stress is reduced significantly and results in a minor transport of bed sediments in the gap; hence, the tunnel erosion stage is then followed by the lee-wake erosion. The lee-wake scour is mainly governed by the vortex shedding and the generated dune at the tunnel erosion stage migrates downstream and ultimately may disappear to form a gentler downstream slope.

The efficiency of a numerical model may depend on its capability to estimate the parameters usually are not possible to be extracted

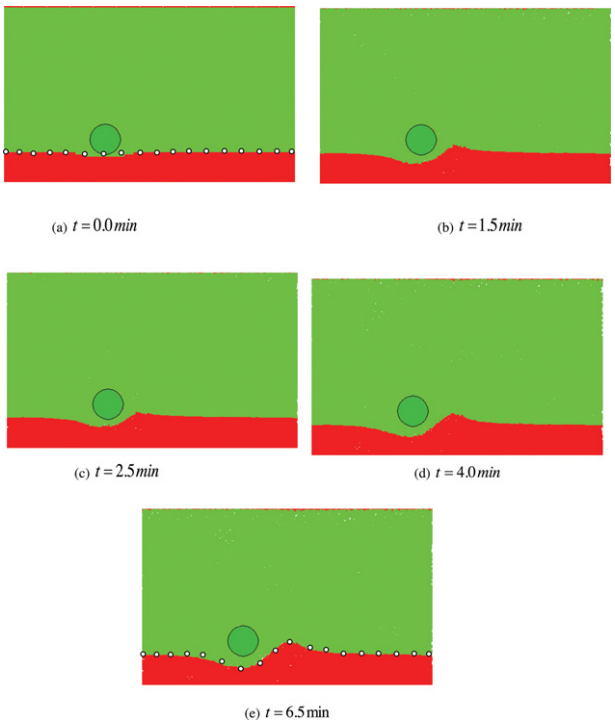

Fig. 10. Snapshots of scour profiles evolution around the pipeline during considered time ($\theta = 0.065$).

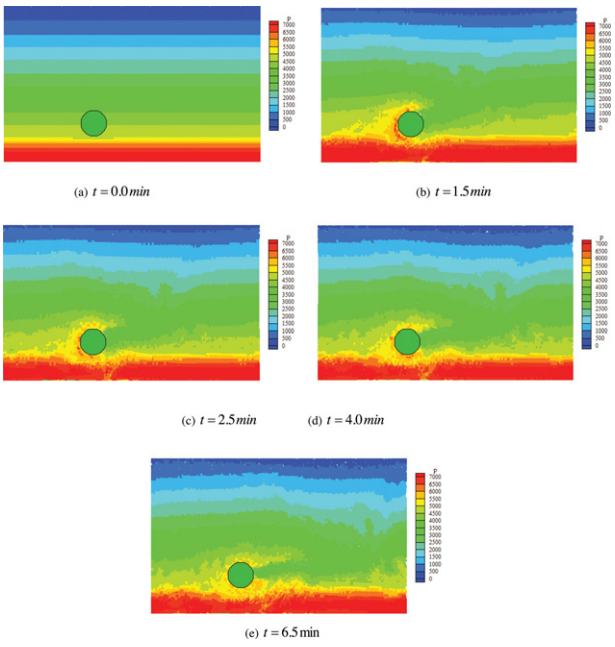

Fig. 11. Pressure distribution around the pipeline in $t = 6.5$ min.

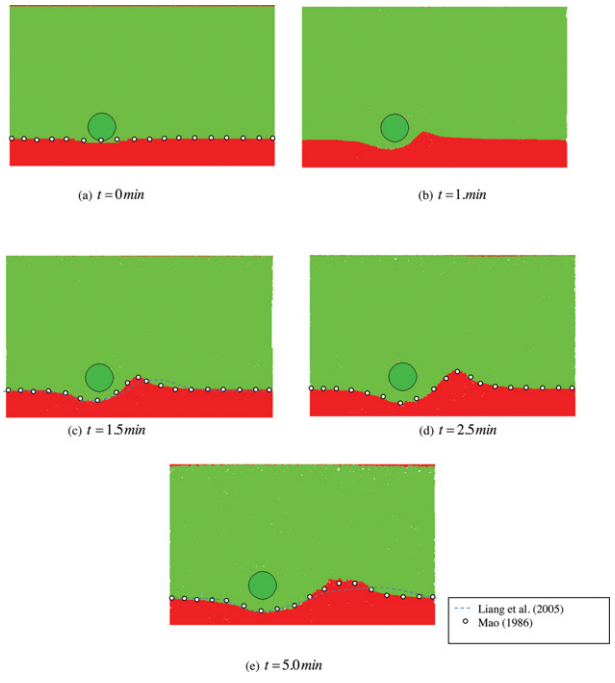

Fig. 12. Snapshots of scour profiles evolution around the pipeline during considered time ($\theta = 0.098$).

from the experimental study. Fig. 11 shows the snapshots of the pressure distribution around the pipe during the early stages of the scour process. The flow pressure is positive and a stagnation point in which maximum pressure is located at the front side of pipe can be detected. But, at the rear side of the pipe due to flow separation, the flow pressure is a great deal less compared to the front side. The figure reveals the effects of a gap flow on the pressure distribution in the scour hole. On the other hand, there is a rapid fall in pressure under the pipe during the scouring process and evolution of scour hole. As expected the pressure in the sediment field is higher because the fluid flow pressure is combined with the sediment particles weight. It may be concluded that the given state equation in the Lagrangian model is capable enough to represent the pressure distribution in both phases. Therefore, this two-phase flow form of the state equation can be used to capture the pressure fields, while the fluid–sediment interaction terms may also play a constructive role in the numerical stability of model.

For the second case, the Lagrangian coupling two-phase model was compared with the Shields parameter of $\theta = 0.098$ case. After execution for about 5 min, the scour profile's evolution is reported in Fig. 12. To have a better comparison, the result of Liang et al. [10] as a single phase model is also presented in the figure with a dashed line. As can be readily seen from the figure, the obtained profiles from the two-phase flow model are identical to the registered profiles of Mao's experiment. The scour profiles in Fig. 12(d) and (e) (at $t = 2.5$ min and $t = 5.0$ min) indicated the superior capability of the Lagrangian two-phase model to handle the accretion of sediment behind the pipe compare to the initial stage of scour development for the live-bed scour cases. Furthermore, the momentum transformation between fluid and sediment phases can be taken into account by the considered interaction terms in Eq. (18). Based on the authors' experience, the considered drag force shows that the closer fluid particles transfer more momentum to the sediment particles by using the kernel function characteristic.

One of the important parameter in investigating the scour at the early stages, which is very difficult to measure, is the sediment transport rate in the scour gap beneath a pipe. The non-dimensional sediment transport rate φ_t in the scour gap was estimated as follows:

$$\phi_t = \frac{q_s}{\sqrt{(S-1)gd^3}} \tag{42}$$

where q_s is the non-dimensional sediment rate in the gap and S is the relative specific gravity of the sediment particles ($=\rho_s/\rho_f$). The time variation of the non-dimensional transport rate is presented in Fig. 13. Some fluctuations can be observed in the transport rate, which is attributed to the SPH model characteristics; the trend of transport

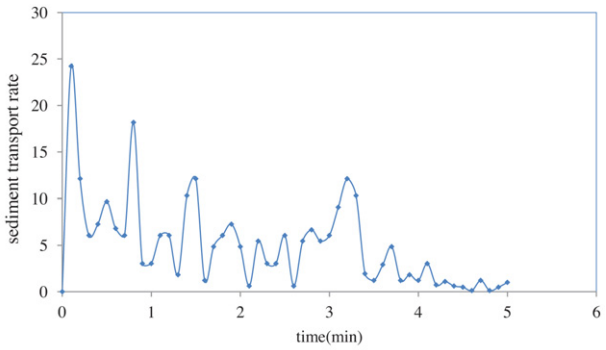

Fig. 13. Time-averaged non-dimensional sediment transport rate under the pipeline.

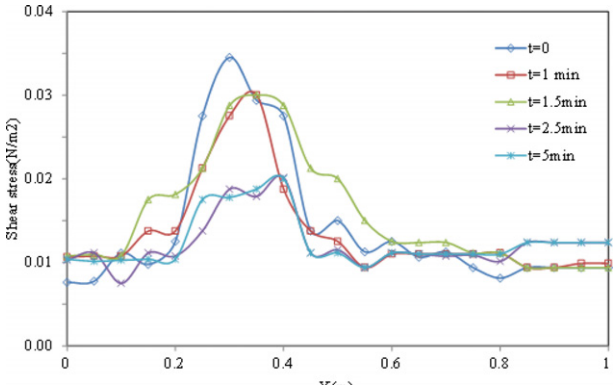

Fig. 14. Time-averaged shear stress near the movable bed from $t = 0$ min till $t = 5$ min.

rate, however, can be clearly traced. As seen from the figure, a violent transport rate is observed with the maximum value of transport flux increases as the scour hole is expanding at the initial stages of the tunnel erosion. The non-dimensional transport rate then gradually decreased with time. It may be concluded that the upstream part of the scour hole was generated quickly during the tunnel erosion stage [12]. After the scour gap develops enough, a minor transport rate can be observed in the gap; hence, the tunnel erosion stage is then followed by early stage of the lee-wake erosion.

On the other hand, reduction in the transport rate may be attributed to the decreases in bottom shear stress in the gap. Fig. 14 shows the estimated bottom shear stress in the scour gap beneath the pipe at $t = 0.0$, 1.0, 1.5, 2.5 and 5 min. As expected, at the beginning of tunnel erosion the bottom shear stress increases significantly due to large velocity in the gap beneath the pipe, while, the bottom shear stress is almost constant at the far upstream and downstream sides of the pipe. This huge shear stress results in intensive sediment transport in the gap, as a result the sediment dune forms at the rear side of pipe. After the scour gap develops enough, the fluid shear stress is decreased drastically and a minor sediment transport rate is induced in the gap beneath the pipe; hence, it is apparent the tunnel erosion stage is almost completed and the early stage of the lee-wake erosion is started. This finding is in agreement with the experimental results of Mao [1] and also shows the model capability to simulate current-induced scour for both the tunnel erosion and starting stage of lee-wake erosion.

5. Conclusive remarks

In this paper, the scour beneath a pipeline as a significant factor in design of pipelines was investigated by a new Lagrangian coupling two-phase flow model. In the Lagrangian model the Smoothed Particle Hydrodynamics (SPH) capability was employed to simulate sediment and fluid particles movement, respectively as the Newtonian and non-Newtonian fluids. The SPS turbulence model is closured to the fluid phase to simulate the fluid turbulence; while, a soft contact approach is employed in the sediment phase to estimate the interparticle collision forces. Furthermore, the fluid–sediment interactions were imposed by drag force, pressure gradient and viscosity terms based upon the Newtonian third law. Sediment viscosity also in terms of its non-Newtonian fluid behavior was taken into account by Cross rheology. The model capability was implemented to simulate the current-induced live bed scour beneath a pipe at the tunnel erosion and the early stage of lee-weak erosion. The model efficiency was compared versus the Mao [1] and Oner et al.'s [24] experiments. This led to the complete simulation of tunnel erosion along with the initial stages of lee-weak scouring. The following conclusions can be drawn from the present study:

- The Lagrangian coupling two-phase flow model is a capable approach for predicting the current-induced live bed scour profile at the tunnel erosion and early stage of lee-weak erosion.
- The bottom shear stress increases significantly at the start of the tunnel erosion that results in a violent transport flux in the scour hole at the tunnel erosion. It then gradually decreased with time due to large velocity in the gap beneath the pipe. Therefore the upstream part of the scour hole is generated quickly during the tunnel erosion stage.
- After the scour gap develops enough, a minor transport rate can be observed in the gap; hence, the tunnel erosion stage is then followed by early stage of the lee-wake erosion. This finding is in agreement with the experimental results.
- Finally, it should be pointed out that the study presented in this paper is limited in the following aspects: (i) the viscous and drag force term introduced in Eqs. (11) and (16) were not radial and hence might not conserve the linear and angular momentum. Conservation of linear and annular momentum may play an important role in the particle-based methods such as the SPH method [40,41,42,43]. (ii) The model execution is rather time-consuming; to overcome this drawback a parallel computing code is essential. These improvements would be the goal of future studies.

Acknowledgments

The first author would like to express his gratitude to Deputy of Research, Iran University of Science and Technology (IUST) for the partial support to his research work. Also the authors would like to thank the reviewers for their constructive and thorough comments, which have led to improvements in this paper.

References

[1] Mao Y. The interaction between a pipeline and an erodible bed. Series Paper 39. PhD dissertation. Lyngby: Tech. Univ. of Denmark.
[2] Kjeldsen SP, Gjø rsvik O, Bringaker KG, Jacobsen J. Local scour near offshore pipelines. Proc. ocean engineering under arctic conditions conference. University of Iceland; 1973, p.308–331.
[3] Lucassen RJ. Scour underneath submarine pipelines. MATs Rep. The Netherlands: PL-4 2A Marine Tech. Res.; 1984.
[4] Sumer BM, Fredsø e J. The Mechanics of Scour in the Marine Environment. World Scientific Singapore. 2002:536 pp.
[5] Subhasish D, Navneet PN. Clear-water scour below underwater pipelines under steady flow. Journal of Hydraulic Engineering, ASCE. 2008:588–600.
[6] Chao JL, Hennessy PV. Local scour under ocean outfall pipelines. Journal of the Water Pollution Control Federation. 1972;44(7):1443–1447.
[7] Hansen EA, Fredsø e J, Ye M. Two-dimensional scour below pipelines. In: Proc 5th int. symp. on offshore mech. and arctic eng.;1986:670-678.
[8] Li F, Cheng L. A numerical model for local scour under offshore pipelines. Journal of Hydraulic Engineering. 1999;125:400–406.

[9] Brørs B. Numerical modeling of flow and scour at pipelines. Journal of Hydraulic Engineering. 1999;125:511–523.
[10] Liang D, Cheng L, Li F. Numerical modeling of flow and scour below a pipeline in currents. Part II. Scour simulation. Coastal Engineering. 2005;52:43–62.
[11] Leeuwenstein W, Bijker EA, Peerbolte EB, Wind HG. The natural self-burial of submarine pipelines. Proc. 19th IASTED international conference modeling and simulation (BOSS) Elsevier; 1985, vol. 2.
[12] Yeganeh-Bakhtiary A, Kazeminezhad MH, Etemad-Shahidi A, Bass J, Cheng L. Euler–Euler two-phase flow simulation of tunnel erosion beneath marine pipelines. Journal of Applied Ocean Research. 2011;33(1):137–146.
[13] Zhao Z, Fernando H. Numerical simulation of scour around pipelines using an Euler-Euler coupled two-phase model. Journal of Environmental Fluid Mechanics. 2007;7(22):121–142.
[14] Amoudry LO, Liu PLF. Two-dimensional two-phase granular sediment transport model with application to scouring downstream of an apron. Coastal Engineering. 2009;56(7):693–702.
[15] Kazeminezhad MH, Yeganeh-Bakhtiary A, Etemad-Shahidi A, Bass J. Two-phase simulation of wave-induced tunnel scour beneath marine pipeline. Journal of Hydraulic Engineering ASCE. 2012;138(1):517–529.
[16] Yeganeh AB, Gotoh H, Sakai T. Applicability of Euler–Lagrange coupling multiphase flow to bed-load transport under high bottom shear. Journal of Hydraulic Research. 2000;38(6):389–398.
[17] Yeganeh-Bakhtiary A, Shabani M, Gotoh H, Wang SM. A three-dimensional distinct element model for bed-load transport. Journal of Hydraulic Research. 2009;47(2):203–212.
[18] Yeganeh-Bakhtiary A, Zanganeh M, Kazemi E, Cheng L, Abd Wahab AK. Euler–Lagrange two-phase model for simulating live-bed scour beneath marine pipelines. Journal of Offshore Mechanics and Arctic Engineering ASCE, DOI:OMAE-10 1095; in press.
[19] Lucy LB. Numerical approach to testing the fission hypothesis. Astronomical Journal. 1977;82:1013–1024.
[20] Monaghan JJ. Smoothed particle methods for hydrodynamics. Computer Physics Report. 1985;3:71–124.
[21] Ha HB, Sako K, Fukagawa R. Numerical simulation of soil–water interaction using smoothed particle hydrodynamics (SPH) method. Journal of Terramechanics. 2007;44:339–346.
[22] Gotoh H, Shao S, Memita T. SPH-LES model for numerical investigation of wave interaction with partially immersed breakwater. Coastal Engineering. 2004;46(1):39–63.
[23] Cundall PA, Strack OD. A discrete numerical model for granular assembles. Geothectiuqe. 1979;29(1):511–523.
[24] Oner A, SalihKirkgoz M, M Sami Akoz. Interaction of current with circular cylinder near rigid bed. Ocean Engineering. 2008;35:1492–1504.
[25] Gotoh H, Sakai T. Key issues in the particle method for computation of wave breaking. Coastal Engineering. 2006;53(2–3):171–179.
[26] Gotoh H, Hayashi M, Sakai T. Refined solid-phase model in Lagrangian particle method for solid-liquid two-phase-flow-none-Newtonian solid-phase model with multi-scale link for graded sediment. Proc. of ICHE-2004; 2004 [on CD].
[27] Ting ST, Prakash M, Clearly PW, Thompson MC. Simulation of high Reynolds number flow over a backward facing step using SPH technical report. CSIRO; 2005, p.292–309.
[28] Colagrossi A, Landrini M. Numerical simulation ofinterfacial flows by Smoothed Particle Hydrodynamics. Journal of Computational Physics. 2003;191:448–475.
[29] Khayyer A, Gotoh H. Modified moving particle semi-implicit methods for the prediction of 2D wave impact pressure. Coastal Engineering. 2009;56(4):419–440.
[30] Khayyer A, Gotoh H. A higher order Laplacian model for enhancement and stabilization of pressure calculation by the MPS method. Applied Ocean Research. 2010;32(1):124–131.
[31] Khayyer A, Gotoh H. Enhancement of stability and accuracy of the moving particle semi-implicit method. Journal of Computational Physics. 2011;230(8):3093–3118.
[32] Sibilla S. A SPH-Based method to simulation local scouring. Proc. 19th IASTED international conference modeling and simulation. 2008.
[33] Barnes HA, Hutton JF, Walters K. An introduction to rheology. Elsevier Science Publishers; 210 pp; 1989.
[34] Shao SD, Edmond YM. Incompressible SPH method for simulating Newtonian and non- Newtonian flow with a free surface. Advanced in Water Resources. 2003;26(1):787–800.
[35] Liang D, Cheng L. Numerical modeling of flow and scour below a pipeline in currents. Part I. Flow simulation. Coastal Engineering. 2005;52:25–42.
[36] Zou S. Coastal sediment transport simulation by Smoothed Particle Hydrodynamics. PhD dissertation. The Johns Hopkins University; 2007.
[37] Monaghan JJ, Kos A. Solitary waves on a Creta beach. Journal of Waterway, Port, Coastal, and Ocean Engineering. 1999;68:1703–1759.
[38] Morris JP, Fox PJ, Shu Y. Modeling lower Reynolds number incompressible flows using SPH. Journal of Computational Physics. 1997;136:214–226.
[39] Issa R, Lee ES, Violeau D. Incompressible separated flows simulations with Smoothed particle hydrodynamics gridless method. International Journal for Numerical Methods in Fluids. 2005;47:1101–1106.
[40] Bonet J, Lok TSL. Variational and momentum preservation aspects of Smooth Particle Hydrodynamic formulations. Computer Methods in Applied Mechanics and Engineering. 1999;180:97–115.
[41] Khayyer A, Gotoh H, Shao SD. Corrected incompressible SPH method for accurate water-surface tracking in breaking waves. Coastal Engineering. 2008;55:236–250.
[42] Vaughan GL, Healy TR, Bryan KR. Completeness, conservation and error in SPH for fluids. International Journal for Numerical Methods in Fluids. 2008;56(1):37–62.
[43] Khayyer A, Gotoh H, Shao SD. Enhanced predictions of wave impact pressure by improved incompressible SPH methods. Applied Ocean Research. 2009;31(2):111–131.